

# Supplementary Information

## UV-C decontamination for N95 emergency reuse: Quantitative dose validation with photochromic indicators

Alison Su<sup>1,2,3‡</sup>, Samantha M. Grist<sup>1,3‡</sup>, Alisha Geldert<sup>1,2,3</sup>, Anjali Gopal<sup>1,2,3</sup>, and Amy E. Herr<sup>1,2,3,4\*</sup>

<sup>1</sup>Department of Bioengineering, University of California, Berkeley

<sup>2</sup>UC Berkeley – UCSF Graduate Program in Bioengineering, Berkeley, United States

<sup>3</sup>N95DECON.org

<sup>4</sup>Chan Zuckerberg Biohub, San Francisco, CA

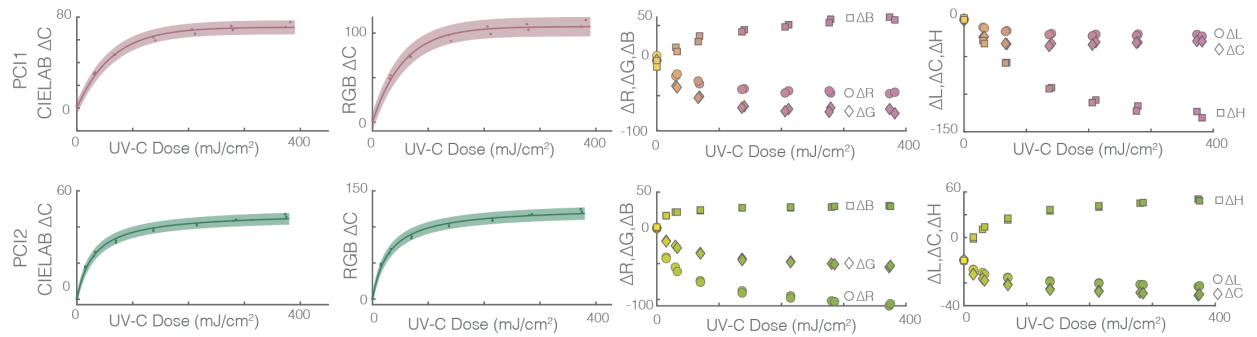
‡These authors contributed equally.

\*Corresponding author: aeh@berkeley.edu

### Table of Contents

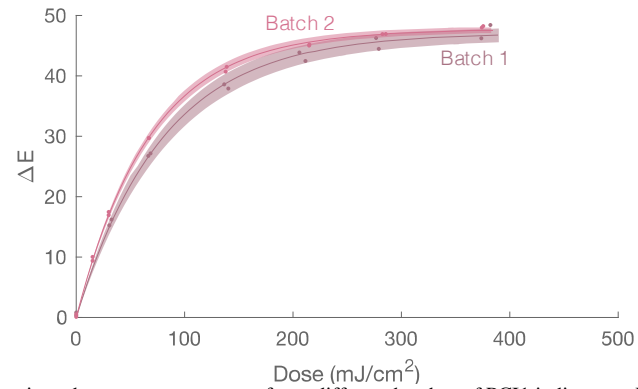
<b>Supplementary Figure S1: Comparison of alternative color difference metrics .....</b>	<b>2</b>
<b>Supplementary Figure S2: PCI1 batch comparison .....</b>	<b>3</b>
<b>Supplementary Figure S3: Comparison of calibration fit functions for PCI2 .....</b>	<b>4</b>
<b>Supplementary Figure S4: Assessing PCI sensitivity to non-germicidal UV-C wavelengths .....</b>	<b>5</b>
<b>Supplementary Figure S5: Radiometer correction factor .....</b>	<b>6</b>
<b>Supplementary Figure S6: Correction factor validation using mask/aperture setup .....</b>	<b>7</b>
<b>Supplementary Figure S7: Correction factor validation using PCIs .....</b>	<b>8</b>
<b>Supplementary Figure S8: Angular response affects quantification of spatial nonuniformity .....</b>	<b>9</b>
<b>Supplementary Figure S9: Physical sensor comparison .....</b>	<b>10</b>
<b>Supplementary Figure S10: Measured on-N95 doses with PCI2 indicators .....</b>	<b>11</b>
<b>Supplementary Figure S11: Quantification uncertainty for imaging using widely available tools .....</b>	<b>12</b>
<b>Supplementary Figure S12: Irradiance variability over time and between systems .....</b>	<b>13</b>
<b>Supplementary Figure S13: Measurement map for characterizing treatment area .....</b>	<b>14</b>
<b>Supplementary Figure S14: Measurement map for on-N95 dose characterization .....</b>	<b>15</b>
<b>Supplementary Table S1. Specifications for robust UV-C measurements .....</b>	<b>16</b>
<b>Supplementary Table S2: Quantified on-N95 doses .....</b>	<b>17</b>
<b>Supplementary Note 1: Informed UV-C system design and validation PCI workflow example ...</b>	<b>18</b>
<b>Supplementary Note 2: Comparison of color difference metrics .....</b>	<b>20</b>
<b>Supplementary Note 3: Generation of PCI calibration functions .....</b>	<b>21</b>
<b>Supplementary Note 4: Assessing specificity of PCIs to germicidal UV-C .....</b>	<b>23</b>
<b>Supplementary Note 5: Radiometer correction factor determination .....</b>	<b>24</b>
<b>Supplementary Note 6: Correction factor validation using a mask/aperture setup .....</b>	<b>26</b>
<b>Supplementary Note 7: Nonuniformities in and between UV-C sources necessitate rigorous UV-C dose characterization .....</b>	<b>27</b>
<b>References .....</b>	<b>28</b>

**Supplementary Figure S1: Comparison of alternative color difference metrics**



**Supplementary Figure S1.** Plots of alternate color difference metrics for PCI1 and PCI2, as a function of UV-C exposure dose. From left, the CIELAB 1976  $\Delta C$  (Euclidean), RGB Euclidean  $\Delta C$ , differences in each RGB component, and differences in each LCH component, are plotted for each PCI type. Differences in RGB and LCH components are plotted in the measured sensor color; 95% prediction intervals are plotted as the shaded regions on CIELAB and RGB  $\Delta C$ .

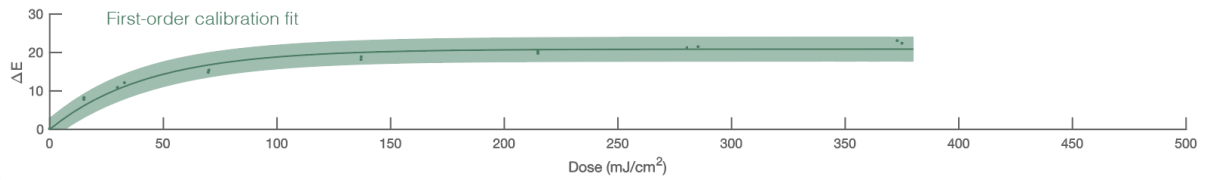
## Supplementary Figure S2: PCI1 batch comparison



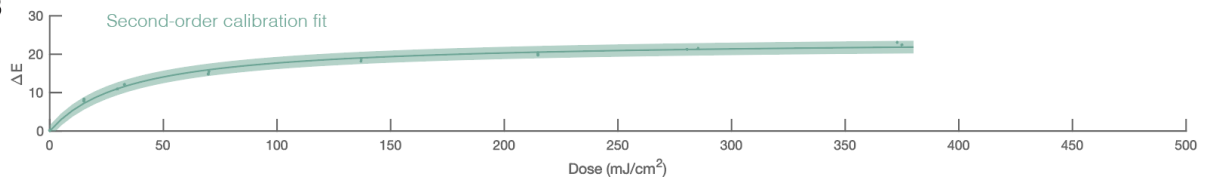
**Supplementary Figure S2.** Comparison dose-response curves of two different batches of PCI1 indicators. For batch 1,  $R^2 = 0.9976$ ,  $a = 47.1$  (46.1, 48.1),  $b = 74.6$  (74.6, 86.3). For batch 2,  $R^2 = 0.9994$ ,  $a = 47.7$  (47.3, 48.2),  $b = 68.6$  (66.3, 70.8). Slight differences in dose-response data may be due to different batches of indicator, different environmental conditions and systems for UV-C exposure (all batch 2 sensors were exposed in System 1 whereas half of the batch 1 data were exposed in System 2), and potentially indicator color change during storage.

### Supplementary Figure S3: Comparison of calibration fit functions for PCI2

**A**

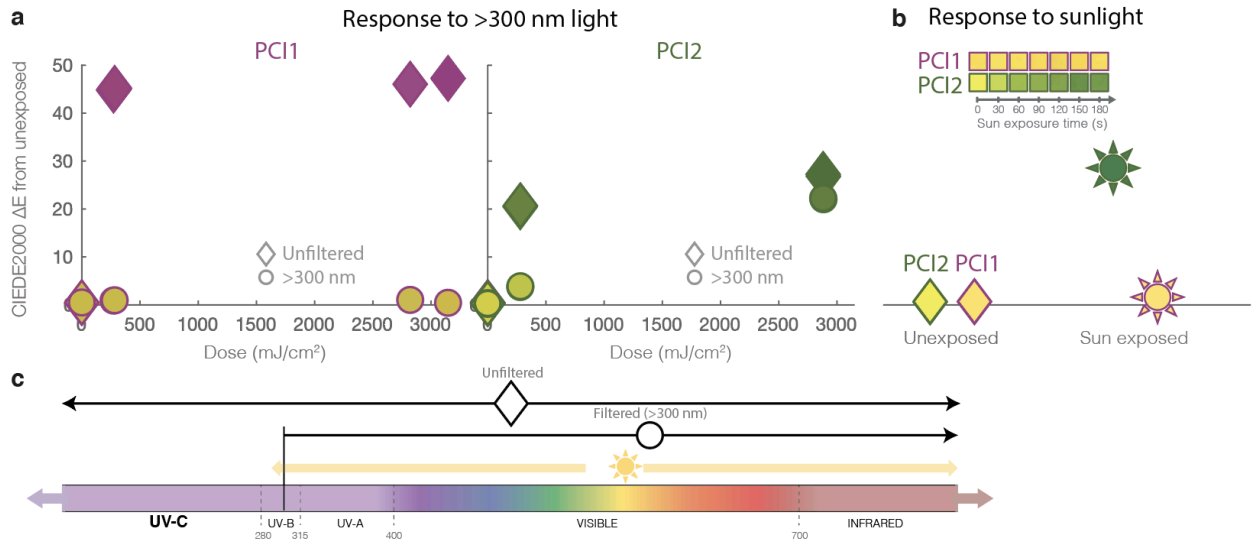


**B**



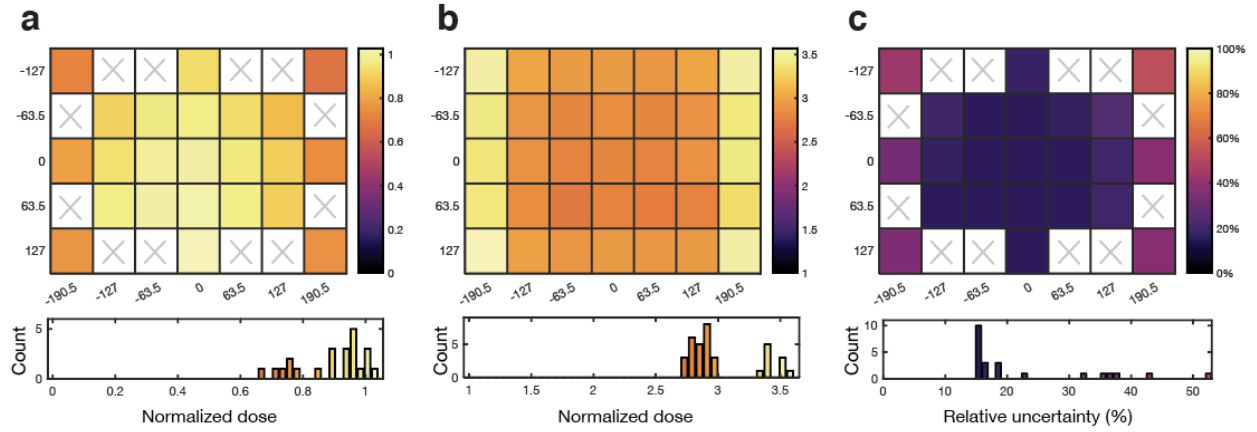
**Supplementary Figure S3.** Comparison of calibration fit functions based on first-order reaction kinetics (a) and second-order reaction kinetics (b) for PCI2. Using the second-order reaction kinetics results in better fit and smaller confidence intervals. For the first-order fit (a),  $R^2 = 0.967$ ,  $a = 20.9$  (19.7, 22.0),  $b = 43.0$  (33.5, 52.6). For the second-order fit (b),  $R^2 = 0.992$ ,  $a = 47.7$  (45.9, 49.5),  $b = 0.00060$  (0.00049, 0.00072). In each plot, fitted data are represented as points, best fit lines are represented as solid lines, and 95% prediction intervals are plotted as shaded regions on each plot.

**Supplementary Figure S4: Assessing PCI sensitivity to non-germicidal UV-C wavelengths**



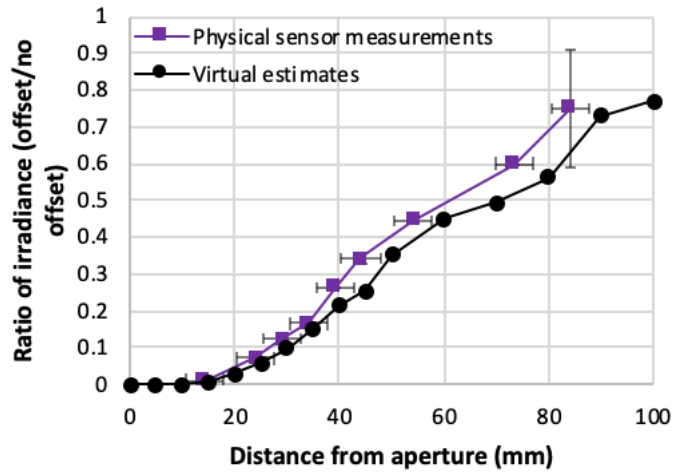
**Supplementary Figure S4.** PCI quantification workflow reveals model-dependent indicator specificity to germicidal UV-C. (a) Comparing responses from bare, unfiltered indicators (diamonds) to those underneath a longpass filter (circles; blocking light below 300 nm) quantifies the sensitivity of PCIs to >300 nm light. Dose axis denotes unfiltered 254 nm UV-C dose measured with the OAI radiometer. (b) Quantified color change after sun exposure of the indicators outdoors assesses indicator sensitivity to sunlight. Pink symbol outlines correspond to PCI1, green symbol outlines refer to PCI2. Symbol fill color depicts the sensor color of each measurement (yellow shows minimal color change; pink or green shows color change). (c) Schematic showing the relevant portion of the electromagnetic spectrum and the relevant wavelengths associated with the filtered and unfiltered measurements and sunlight.

**Supplementary Figure S5: Radiometer correction factor**



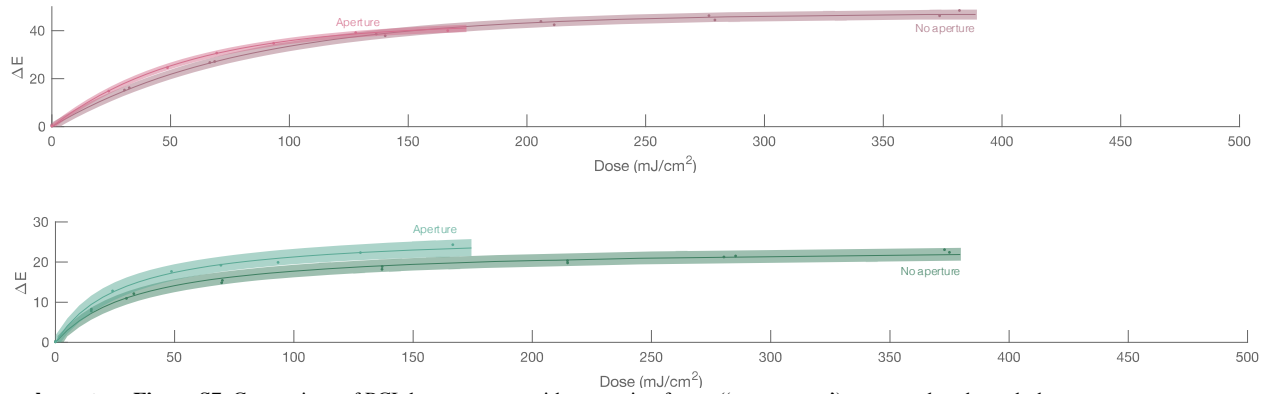
**Supplementary Figure S5.** Heatmaps depicting the (a) ratio between normalized (to the maximum reading) readings of the radiometer and the virtual sensor. (b) spatially varying radiometer correction factor, and (c) the spatially dependent relative uncertainty associated with the correction factor.

**Supplementary Figure S6:** Correction factor validation using mask/aperture setup



**Supplementary Figure S6.** Validation of modelled virtual calibration factor approach: comparison between modelled and measured irradiances at varying distances from the aperture. This was one of the validation measurements performed for the virtual calibration factor, as described in Supplementary Note 6. Vertical error bars show error-propagated standard deviation of N=3 measurements. Horizontal error bars depict propagated error in height measurements.

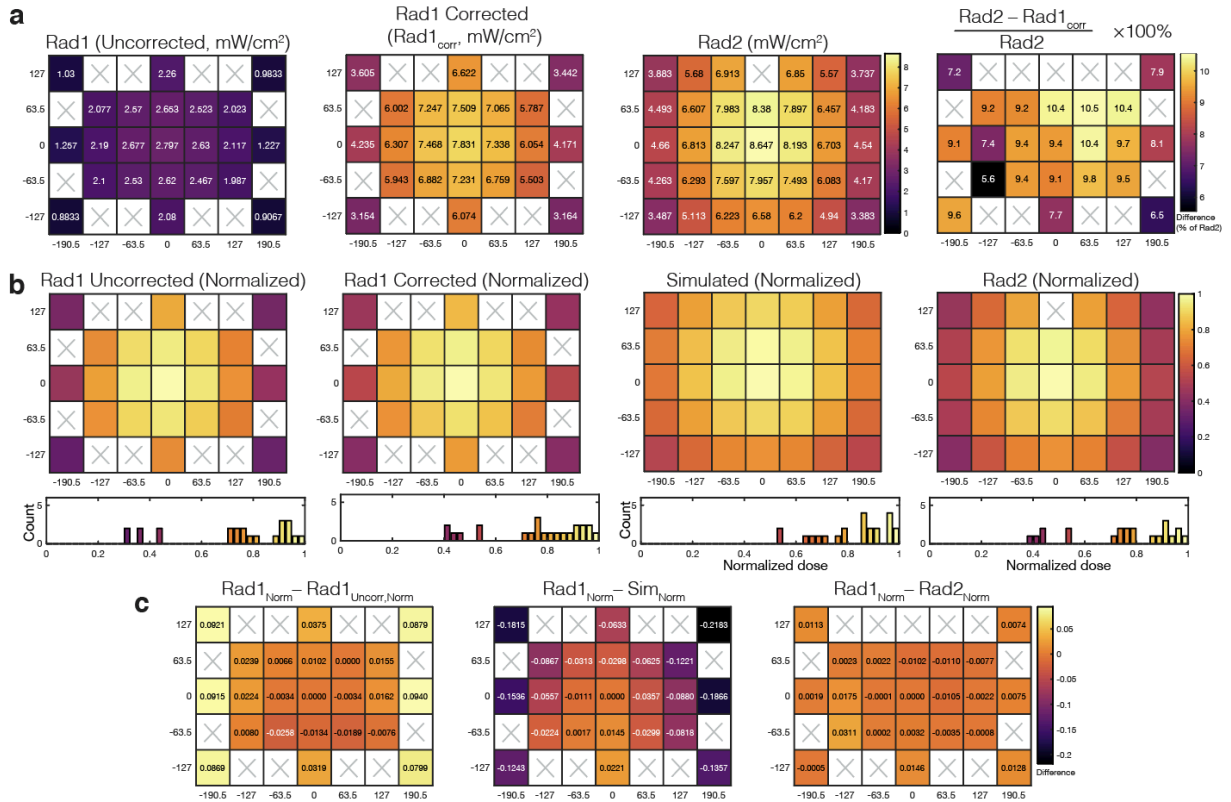
### Supplementary Figure S7: Correction factor validation using PCIs



**Supplementary Figure S7.** Comparison of PCI dose response with correction factor ('no aperture') compared to through the aperture ('aperture'), where the estimated correction factor for the OAI radiometer would be 1. This was one of the validation measurements performed for the virtual calibration factor, as described in Supplementary Note 6. Dose-response for PCI1 indicators is shown in the top plot while that for the PCI2 indicators is shown on the bottom.  $R^2$  and fit parameters: (PCI1 no aperture)  $R^2 = 0.998$ ,  $a = 47.1$  (46.1, 48.1),  $b = 80.4$  (74.6, 86.3); (PCI1 aperture)  $R^2 = 0.999$ ,  $a = 42.8$  (41.3, 44.2),  $b = 55.8$  (50.9, 60.6); (PCI2 no aperture)  $R^2 = 0.992$ ,  $a = 47.7$  (45.9, 49.5),  $b = 0.00060$  (0.00049, 0.00072); (PCI2 aperture)  $R^2 = 0.994$ ,  $a = 55.0$  (49.9, 60.0),  $b = 0.00090$  (0.00037, 0.00090). In each plot, fitted data are represented as points, best fit lines are represented as solid lines, and 95% prediction intervals are plotted as shaded regions on each plot.



**Supplementary Figure S8: Angular response affects quantification of spatial nonuniformity.**



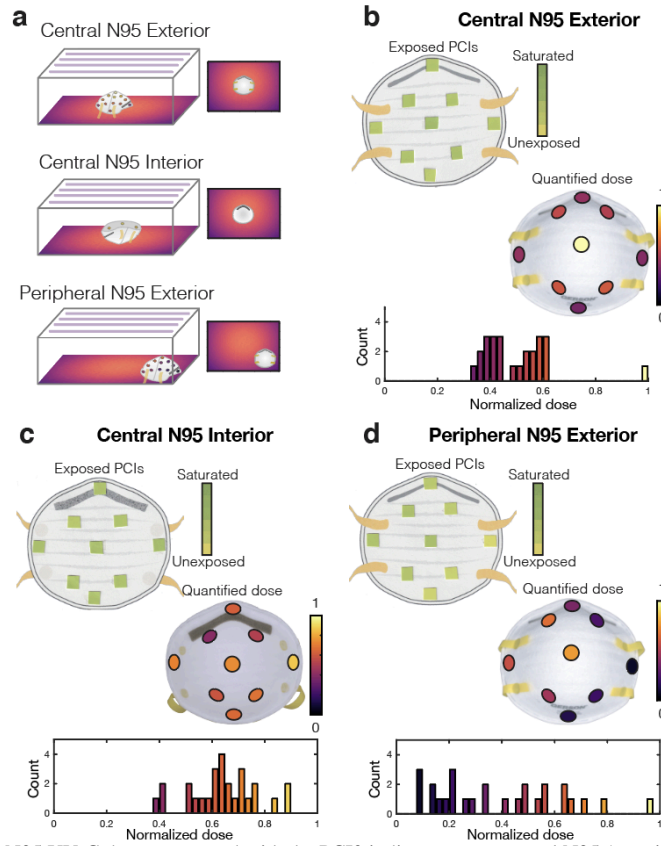
**Supplementary Figure S8.** (a) Two UV-C sensors report ~3X difference in irradiance within the exposure system due to discrepancies in their angular responses (Rad1 has nonideal angular response; Rad2 has near ideal cosine angular response as measured by the manufacturer). Correction of Rad1's angular response with a virtual calibration factor yields irradiance profile in good agreement with Rad2 (within 11% across the treatment plane). (b) Normalized corrected Rad1 measurements agree well with normalized Rad2 measurements and Zemax simulations of the treatment system, although simulations underestimate nonuniformity in irradiance. Each plot shows a heatmap of irradiance values normalized to the center location above a histogram of measured normalized irradiances. (c) Differences between the corrected and uncorrected normalized Rad1 measurements reveal that the uncorrected Rad1 overestimates nonuniformity in irradiance by nearly 10%. Differences between the normalized corrected Rad1 and simulations reveal that simulations underestimate nonuniformity in irradiance by over 20%. Differences between the normalized corrected Rad1 and Rad2 measurements reveals that the corrected Rad1 accurately captures irradiance nonuniformities within 3%. All three heatmaps in (c) plotted on the same scale. White regions with 'x' were not measured. Rad1 is an OAI 308 meter equipped with a 254 nm sensor. Rad2 is an ILT1254/TD radiometer. Each plot depicts the mean of N=3 measurements.

### Supplementary Figure S9: Physical sensor comparison



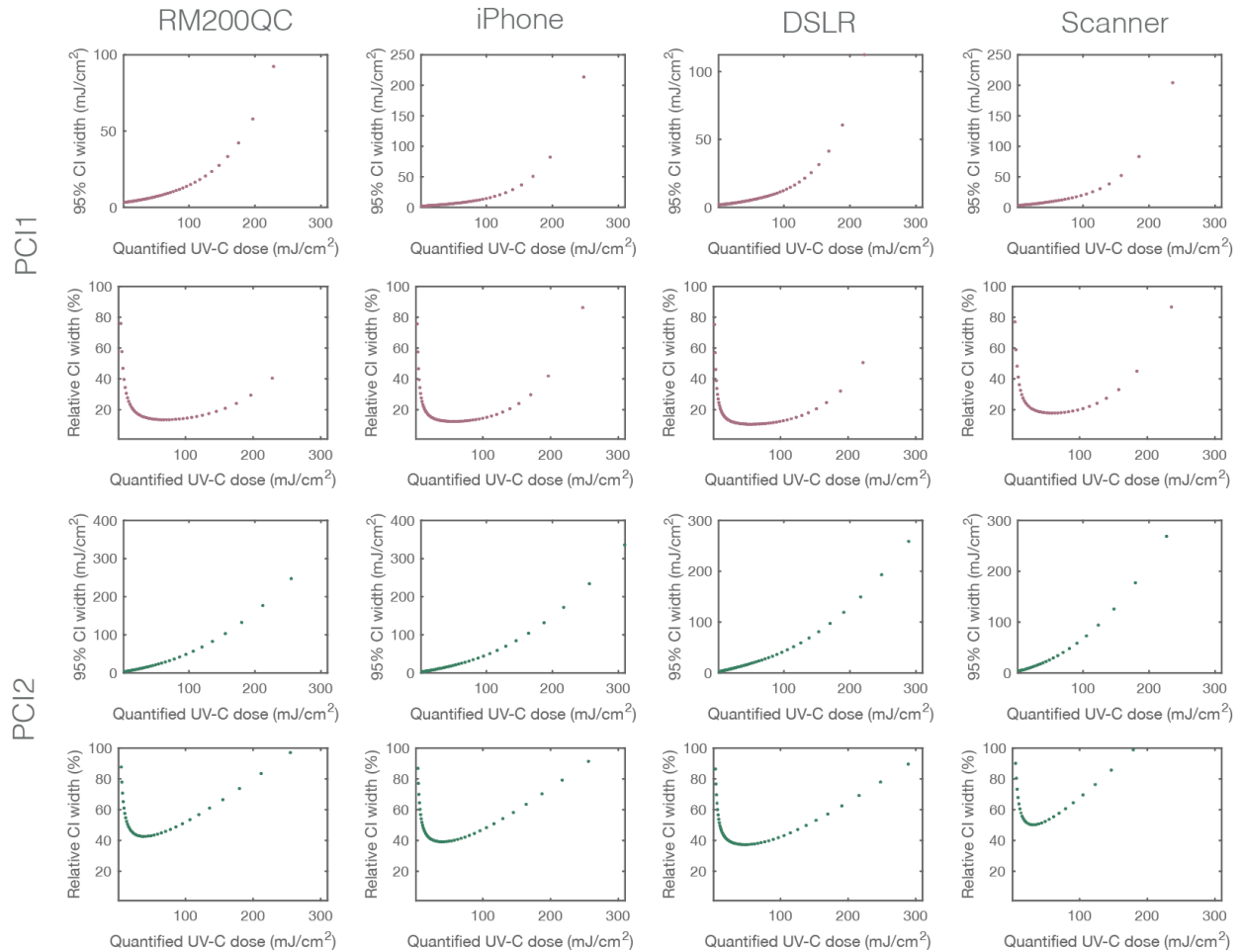
**Supplementary Figure S9.** Comparison of sensors used in this study. From left to right: UVPS photochromic indicator (PC12), Intellego photochromic indicator (PC11), ILT1254 digital radiometer (Rad2), OAI 254 nm sensor (Rad1). PCIs are notably smaller than radiometers, permitting measurement over complex 3D geometries. PCIs are notably smaller than radiometers, permitting measurement over complex 3D geometries.

**Supplementary Figure S10: Measured on-N95 doses with PCI2 indicators**



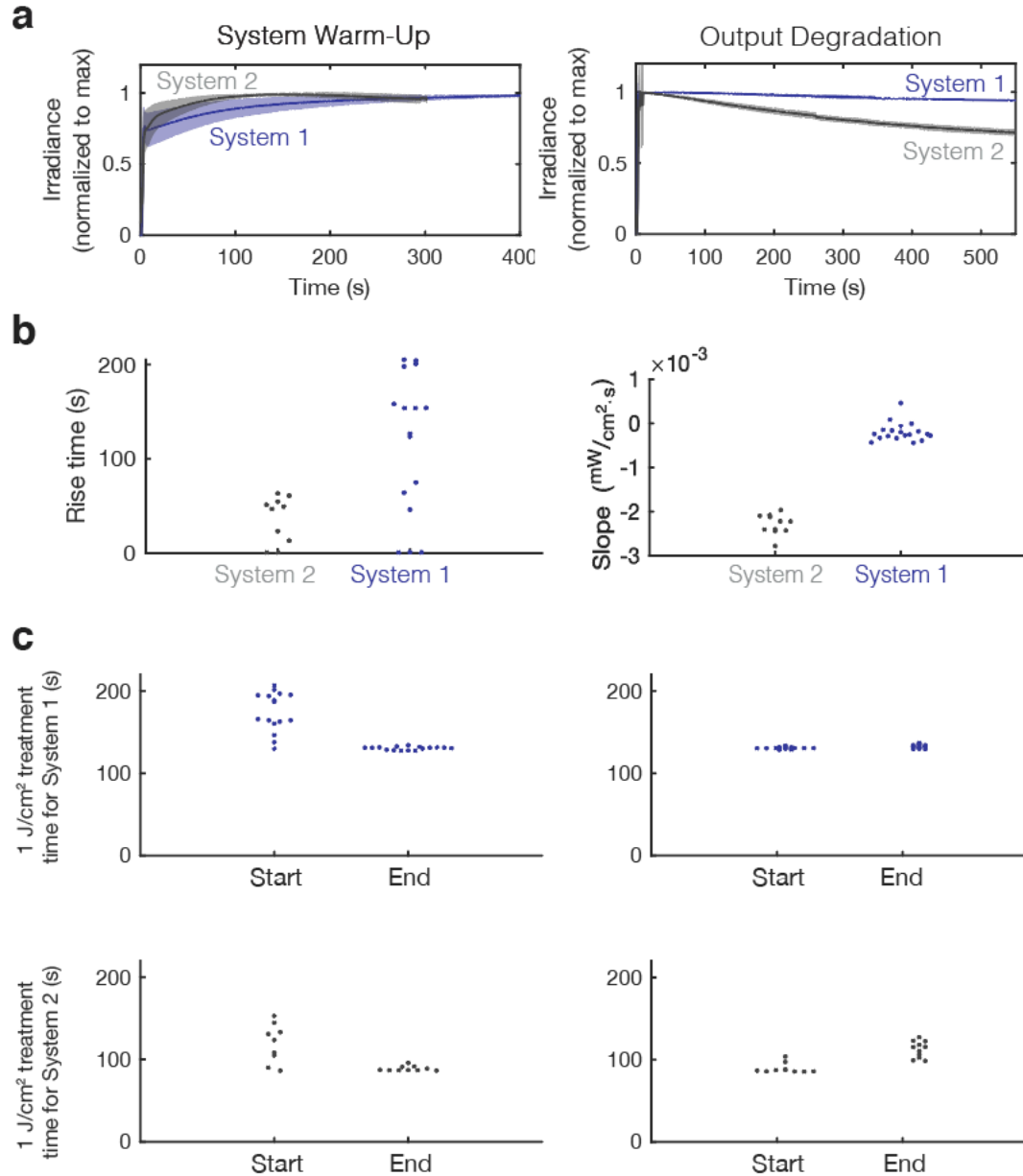
**Supplementary Figure S10.** On-N95 UV-C doses measured with the PCI2 indicators on a central N95 (exterior and interior) and peripheral N95 (equivalent to Figure 3 (a-d) of the main text, but with PCI2 instead of PCI1). (a) On-N95 treatment configurations. (b-d) scanned images of PCIs after exposure (top left), quantified doses (middle right) and histogram of measured doses (bottom) for the three treatment configurations. Scanned images show a representative replicate, on-N95 heatmaps plot the mean of N=3 measurements, while the histograms below each measurement plot all individual measurements.

**Supplementary Figure S11: Quantification uncertainty for imaging using widely available tools**



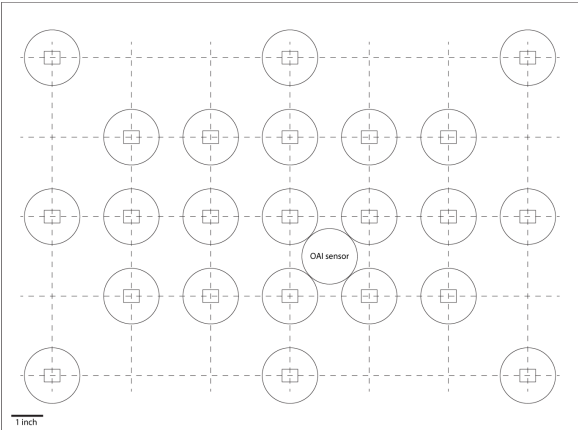
**Supplementary Figure S11.** Absolute and relative widths of 95% confidence intervals on dose measurements from calibration data for the PCI1 (pink) and PCI2 (green) photochromic indicators generated from color differences quantified by widely available imaging tools (calibration curves presented in Figure 4 of the main text). Relative CI widths on a measurement of  $\sim 0.1$  J/cm<sup>2</sup> UV-C dose using the PCI1 indicators are 14.6% for the RM200QC, 15.1% for the iPhone, 12.8% for the DSLR, and 20.8% for the scanner (relative measurement uncertainties of 7.3% for the RM200QC, 7.6% for the iPhone, 6.4% for the DSLR, and 10.4% for the scanner). Relative CI widths on a measurement of  $\sim 0.1$  J/cm<sup>2</sup> UV-C dose using the PCI2 indicators are 53.5% for the RM200QC, 48.4% for the iPhone, 43.3% for the DSLR, and 69.6% for the scanner (relative measurement uncertainties of 26.8% for the RM200QC, 24.2% for the iPhone, 21.7% for the DSLR, and 34.8% for the scanner). While the relative measurement uncertainties of the PCI1 indicators meet the ideal 10% target specifications described in Table S1 for all imaging approaches except the scanner (10.4%), none of the PCI2 measurement uncertainties meet the 10% ideal or 20% marginal targets for a 0.10 J/cm<sup>2</sup> measurement.

**Supplementary Figure S12:** Irradiance variability over time and between systems



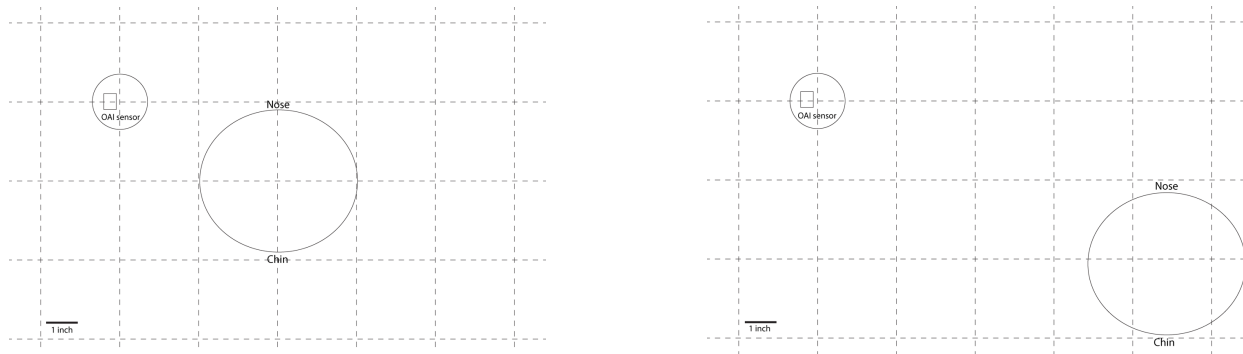
**Supplementary Figure S12.** Validation of UV-C dose is critical for UV-C decontamination due to temporal variations in light output. (a) Figure 5b from the main text depicting measured irradiance during warm-up (left), in which measured irradiance rises with time, and long exposure (right), in which measured irradiance falls with time. (b) Quantification of 10-90% rise time (left) and output degradation slope (right) for multiple exposures in both systems. (c) 1.0 J/cm<sup>2</sup> treatment time estimated from the starting irradiance or ending irradiance for both System 1 (top row) and System 2 (bottom row) in each condition (warmup or long exposure after warmup). For each system, the left minimum treatment time plot corresponds to treatment time computations from an uncontrolled (not necessarily warmed up) start; right plot corresponds to treatment time computations from a warmed-up system.

**Supplementary Figure S13: Measurement map for characterizing treatment plane**



**Supplementary Figure S13.** Map for measurements across the treatment plane using the OAI sensor and the PCIs. Circles depict OAI radiometer positions. Small solid rectangles depict PCI placement. Circle labelled 'OAI sensor' depicts OAI radiometer location during PCI exposure.

### Supplementary Figure S14: Measurement map for on-N95 dose characterization



**Supplementary Figure S14.** Spatial layouts taped to UV-C treatment system floor for consistent N95 respirator and OAI sensor placement. Ellipses depict N95 locations; circle labelled 'OAI sensor' depicts OAI radiometer position during on-N95 measurements. Small solid rectangle above "OAI sensor" depicts PCI placement.

**Supplementary Table S1. Specifications for robust UV-C measurements**

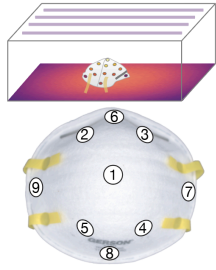
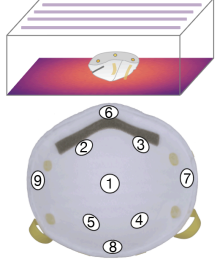
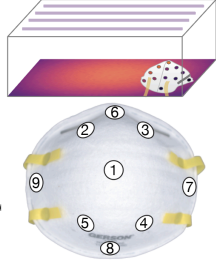
Number	Metric	Units	Marginal value	Ideal value
1	Dose measurement range (in-process validation)	J/cm <sup>2</sup>	> 1.0	> 3.0
2	Dose measurement range (informed design)	J/cm <sup>2</sup>	> 0.1	> 0.3
3	Relative uncertainty on dose measurement (CI)	%	< 20	<10
4	Accuracy	%	> 80	> 90
5	Sensitivity to non-germicidal longer wavelengths	%	< 5	< 1

1. The marginal dose measurement dynamic range for in-process validation ( $\geq 1.0$  J/cm<sup>2</sup>) is based upon the marginally-acceptable dose to be delivered to each and every N95 surface for 3-log inactivation of enveloped viruses (based on peer-reviewed evidence in the scientific literature<sup>1-3</sup>). The measurement method needs to be able to discern whether this dose has been exceeded. Ideally, the measurement range would be higher ( $> 3.0$  J/cm<sup>2</sup>) as the location of the reference sensor during decontamination may receive a higher dose than the N95 surface receiving the lowest dose due to shadowing and the model-dependent angles of the N95 surfaces.
2. Because informed design of N95 decontamination systems and processes can use relative dose measurements, the necessary dose measurement dynamic range for informed design can be lower than that for in-process validation.  $> 0.1$  J/cm<sup>2</sup> was chosen as the marginal value for this application to ensure that the UV-C exposure times for informed design were no less than 1/10<sup>th</sup> those for in-process validation. As informed design uses the same exact UV-C exposure system as that used for the actual decontamination process, low dynamic range PCIs would require very short exposure times because the systems are designed to deliver  $\geq 1.0$  J/cm<sup>2</sup> during a reasonable exposure time. These short exposure times during informed design may (1) not be feasible or (2) introduce unacceptable degrees of run-to-run variability.
3. The calibration uncertainty for very well characterized UV-C radiometers is  $\sim 5\%$ <sup>4</sup> (although many radiometers will not reach this level due to sources of error in UV-C measurements<sup>5</sup>). As measurement solutions like photochromic indicators (PCIs) have advantages over even the best calibrated radiometers (e.g. form factor), we identified a marginal target for PCIs of 4 times the value for radiometers, and an ideal target as twice the radiometer value. These values (20% and 10%, respectively) allow reasonable ‘safety factors’ of  $< 50\%$  to be implemented to ensure minimally-acceptable doses are reached. Safety factors are multipliers on the target dose to take into account uncertainty on the measurements (e.g. for 20% total propagated uncertainty, one may want to use a safety factor of 1.5 and ensure at least  $\geq 1.5$  J/cm<sup>2</sup> was delivered to all N95 surfaces)
4. Accuracy values (how well measurements align with a calibrated, NIST-traceable reference measurement) were chosen to align with target relative uncertainty.
5. Ideally, UV-C measurements for decontamination characterization and validation should only report irradiance/dose within the germicidal range (UV-C extends to 280 nm; germicidal efficacy at 300 nm is  $< 10\%$  of that at 254 nm). We selected marginal and ideal values such that the measurement response to  $> 300$  nm was 1-2 orders of magnitude less than that to  $< 300$  nm light from a commonly employed low-pressure mercury/amalgam source.



## Supplementary Table S2: Quantified on-N95 doses

Supplementary Table S2. Quantified on-N95 relative doses (normalized to the apex location 1 of the exterior of the central respirator) measured with photochromic indicators as depicted in **Supplementary Figure S10** as well as Figure 3 of the main text. Errors are reported as one standard deviation propagated uncertainty encompassing both the standard deviation of 3 replicate measurements (measured across  $\geq 2$  separate days) and the uncertainty on the dose measurement from the calibration curve. Schematics in the left column depict measurement location for each configuration.

Configuration	Location	Norm. Dose (PCI1)	Norm. Dose (PCI2)
Central N95 Exterior 	1	$1.00 \pm 0.08$	$1.00 \pm 0.15$
	2	$0.47 \pm 0.06$	$0.56 \pm 0.08$
	3	$0.38 \pm 0.06$	$0.51 \pm 0.08$
	4	$0.53 \pm 0.07$	$0.61 \pm 0.09$
	5	$0.57 \pm 0.06$	$0.59 \pm 0.09$
	6	$0.36 \pm 0.03$	$0.43 \pm 0.07$
	7	$0.33 \pm 0.03$	$0.39 \pm 0.06$
	8	$0.28 \pm 0.04$	$0.66 \pm 0.06$
	9	$0.38 \pm 0.03$	$0.43 \pm 0.07$
Central N95 Interior 	1	$0.75 \pm 0.07$	$0.74 \pm 0.11$
	2	$0.40 \pm 0.03$	$0.40 \pm 0.06$
	3	$0.48 \pm 0.04$	$0.52 \pm 0.08$
	4	$0.66 \pm 0.07$	$0.68 \pm 0.11$
	5	$0.61 \pm 0.05$	$0.59 \pm 0.09$
	6	$0.60 \pm 0.06$	$0.63 \pm 0.09$
	7	$0.90 \pm 0.07$	$0.87 \pm 0.13$
	8	$0.62 \pm 0.04$	$0.65 \pm 0.10$
	9	$0.73 \pm 0.07$	$0.73 \pm 0.12$
Peripheral N95 Exterior 	1	$0.70 \pm 0.08$	$0.78 \pm 0.19$
	2	$0.65 \pm 0.07$	$0.66 \pm 0.14$
	3	$0.24 \pm 0.03$	$0.25 \pm 0.06$
	4	$0.16 \pm 0.02$	$0.21 \pm 0.03$
	5	$0.43 \pm 0.06$	$0.47 \pm 0.07$
	6	$0.34 \pm 0.04$	$0.37 \pm 0.07$
	7	$0.063 \pm 0.013$	$0.081 \pm 0.018$
	8	$0.104 \pm 0.016$	$0.14 \pm 0.03$
	9	$0.55 \pm 0.07$	$0.58 \pm 0.10$

## Supplementary Note 1: Informed UV-C system design and validation PCI workflow example

As depicted in Figure 1(d) of the main text, in this work we introduce a novel PCI-based dose quantification workflow for UV-C N95 decontamination systems. Step 1 of the workflow involves quantification and calibration of the PCIs. Steps 2-3 involve informed design of UV-C treatment. Step 4 involves in-process validation of every treatment cycle.

**Step 1:** The first step of the workflow is to create a robust calibration curve of PCI color change as a function of dose, using a calibrated, NIST-traceable (or traceable to similar standards organization) radiometer (Figure 1(d, i)). The tested doses should cover the full range of the PCI with sufficient datapoints to yield a well-defined calibration curve fit (we typically acquired data at 7-10 doses), with replicate indicators run at each dose. Color measurements of the PCIs exposed to each dose, along with unexposed and saturated reference indicators, should be acquired immediately (PCI color is often unstable after exposure) with a color measurement tool like a spectrophotometer or spectroradiometer. A more widely-available imaging tool can also be used as long as (1) acquisition parameters are tightly controlled and held constant, (2) raw images are acquired, with the exposed PCI and reference within the same image, (3) the PCIs are isolated from ambient illumination, (4) images are not saturated. Color differences between each PCI and the unexposed reference, as a function of measured UV-C dose, are calculated and fitted to a calibration curve as described in the Methods and Supplementary Note 3. This calibration curve can then be applied to estimate UV-C dose from PCI color change in future experiments. Calibration should be confirmed after changes in condition (e.g. temperature, humidity) and after change in PCI shipment/lot. Example calibration curves are presented in Figure 2 and Figure 4 of the main text.

**Step 2:** After the calibration curve is generated, relative exposures can be mapped across the UV-C treatment plane using either a single exposure of spatially-arrayed PCIs or multiple exposures of a radiometer moved to each position in order to select the best representative N95 and reference positions for on-N95 measurements (Figure 1(d, ii)). To make these measurements, PCIs are placed in defined regions of the treatment plane and exposed to a quantifiable UV-C dose (as determined from the calibration curve of Step 1). UV-C dose at each location is estimated from the calibration curve based on the color difference between each exposed PCI and an unexposed reference PCI using the same acquisition criteria as described in Step 1. Variability around the treatment plane as well as the lowest- and highest-dose regions should be identified at this step, as demonstrated in Figure 2 of the main text. The active area of the treatment plane (area where N95s will ultimately be placed), as well as a reference location within the treatment plane (low-dose region that will not be shadowed by N95s during treatment), should be defined in this step. The inclusion of the reference facilitates translation from informed design to in-process validation in Step 4, when dose may be monitored using only a PCI at the reference location.

**Step 3:** 3D structure adds additional and significant variability to the UV-C dose delivered to N95 surfaces (Figure 1(d, iii)). Steep or shadowed surfaces will receive the lowest dose on a given object, so these regions should be identified on each model of N95 to be decontaminated. PCIs should be placed on these regions as well as regions expected to receive high doses (e.g. N95 apex). Note that the 3D structure, and therefore optimal PCI placement, is expected to be model-dependent (e.g. some models may have pleats that cause shadowing while others may have steeper morphology). To assess the full degree of variability in irradiance to which N95 surfaces may be exposed, representative N95s with PCIs affixed in the expected high and low-dose regions should be placed in the active regions of the treatment plane expected to have (1) the highest dose, and (2) the lowest dose (informed from Step 2). A PCI placed at the reference location during on-N95 measurement enables relative doses delivered to all N95 surfaces to be compared to those at the reference location. PCIs at all locations should be exposed to a UV-C dose within the indicator's quantifiable range. Using the color quantification workflow and calibration curve, relative doses delivered to N95 surfaces in the high and low-dose regions of the treatment plane can then be computed with respect to the dose at the reference location. From this relative dose information, the configuration of N95s within the treatment plane can be optimized (to minimize on-N95 dose variation). Any adjustments to the N95 layout should be reanalyzed to determine the relative dose quantification in the adjusted setup. The minimum dose required at the reference location to ensure all N95 surfaces receive  $\geq 1.0 \text{ J/cm}^2$  should also be assessed. For example, if the lowest-dose N95 region receives 25% of the dose delivered to the reference location, the reference indicator must receive  $\geq 4.0 \text{ J/cm}^2$  in order for all N95 surfaces to receive at least the marginally-effective dose of  $1.0 \text{ J/cm}^2$ . This minimum reference position and dose can then be used for in-process validation of UV-C treatment. An example of on-N95 dose measurement is presented in Figure 3 of the main text.

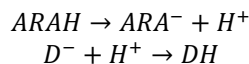
**Step 4:** After identifying the reference indicator location and minimum dose the reference must receive to ensure all surfaces of the N95s receive  $\geq 1.0$  J/cm, an indicator with sufficient dynamic range should be placed at that reference location during each and every UV-C treatment cycle to validate that the minimum reference dose is delivered to the reference location. To extend PCI dynamic range, optical attenuation can be coupled with PCIs (to reduce light reaching the PCI by a known factor, stretching the dynamic range of response to include the minimum reference dose). Examples of optical attenuation are presented in Figure 5 of the main text.

## Supplementary Note 2: Comparison of color difference metrics

Seeking to compare several of the additional metrics of color difference outlined in ASTM D2244-16, we computed and plotted several additional metrics as a function of UV-C dose (**Supplementary Figure S1**)<sup>6</sup>. The RGB and CIELAB  $\Delta C$ , as well as the red and green components ( $\Delta R$ ,  $\Delta G$ ) and the CIE 1976 Metric Hue Difference ( $\Delta H$ ), showed strong dose-dependent response. These dose-dependent relationships suggest that any of these established metrics could be employed for PCI calibration. A previous study characterized an unspecified model of UV Process Supply PCI and defined a color difference metric as  $\Delta R + \Delta G$ ; these previous characterization data appeared to have higher variability than our measurements but with qualitatively similar saturation<sup>7</sup>. Our more robust quantification is likely due to (1) our use of a dedicated, contact color measurement tool instead of a camera<sup>8,9</sup> and (2) our direct, logged measurements of UV-C dose to generate the calibration curve rather than modelled irradiance. As the CIEDE2000 metric<sup>10</sup> showed comparable dose-response to the other metrics and has been found to better correlate with perceptible color difference and outperform other color difference standards<sup>11,12</sup>, we chose to employ CIEDE2000  $\Delta E$  as the color difference metric for subsequent calibration and measurement in our characterization and application of the PCIs.

### Supplementary Note 3: Generation of PCI calibration functions

We endeavored to define a calibration function mapping the color change of photochromic UV-C indicators to quantitative UV-C dose (fluence). For some types of UV indicator<sup>13</sup>, the sensing mechanism involves one molecule (acid-release agent, ARAH) that is triggered by UV light to release a proton (H<sup>+</sup>), which then protonates another dye molecule (D<sup>-</sup>), resulting in a color change:



To design an appropriate calibration function to which to fit color change data (CIEDE2000<sup>10</sup> color differences from an unexposed sensor) as a function of UV dose (*dose*), we hypothesized that, depending on rate-limiting step of the reaction, one might be able to use functions based on expected product concentration from first- or second-order reaction kinetics. For first-order reaction kinetics<sup>14</sup>:

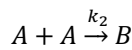


$$[B] = [A]_0 \{1 - e^{-k_1 t}\}$$

Assuming the color change is proportional to the concentration of product, and using the relationship that *dose* = *irradiance* · *t*:

$$\Delta E \approx a \left\{ 1 - e^{-\frac{\text{dose}}{b}} \right\}$$

Where  $b \equiv \text{irradiance}/k_1$ . We found that this first-order kinetics fit function fit the PCI1 color change data well. However, we noted that the fit was poorer for PCI2, with lower goodness-of-fit and poor visual agreement (as depicted in **Supplementary Figure S3**). We hypothesized that a fit function derived from second-order reaction kinetics might yield better fit performance for the PCI2 model. As a first pass, we chose the simplest type of second-order reaction<sup>14</sup>:



$$\frac{1}{[A]} = \frac{1}{[A]_0} + k_2 t$$

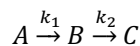
$$[A] = \frac{[A]_0}{1 + [A]_0 k_2 t}$$

$$[B] = \frac{[A]_0 - [A]}{2} = \frac{[A]_0 \left\{ 1 - \frac{1}{1 + [A]_0 k_2 t} \right\}}{2} = \frac{\frac{1}{2} [A]_0^2 \cdot k_2 t}{1 + [A]_0 k_2 t}$$

$$\Delta E \approx \frac{\frac{1}{2} a^2 \cdot b \cdot \text{dose}}{1 + a \cdot b \cdot \text{dose}}$$

This function based on second-order reaction kinetics better fits the PCI2 data, as depicted in **Supplementary Figure S3**.

Due to the two-stage reaction described by Mills, *et al.*, it may be more relevant to use an equation derived from consecutive first-order reactions<sup>14</sup>:



$$[C] = [A]_0 \left\{ 1 + \frac{1}{k_1 - k_2} [k_2 e^{-k_1 t} - k_1 e^{-k_2 t}] \right\}$$

$$\Delta E \approx c \left\{ 1 + \frac{1}{a - b} [b e^{-a \cdot \text{dose}} - a e^{-b \cdot \text{dose}}] \right\}$$

However, when this equation was applied to data from PCI1, the fitting algorithm could not robustly quantify all three fit parameters (with 10 points fitted and  $R^2=0.9993$ ; the 95% CI on fit parameter  $b$  extended from  $-1.3E+08$  to  $1.3E+08$ ). This was likely because fit parameter  $a$  (0.001398) was found to be much smaller than fit parameter  $b$  (2328), suggesting that the color change is limited by one of the constituent reactions (and thus may be approximated as a single first-order reaction). Similarly, when the fit was applied to PCI2, the second fit parameter was again poorly defined and the goodness-of-fit similar to that for the equation based on a single first-order reaction.

After fitting the calibration function to the CIEDE2000 vs. UV-C dose data, 95% confidence prediction bounds on the fit were generated using the MATLAB® 'predint' function, generating non-simultaneous observation bounds. The upper bound of this prediction interval, with the addition of a safety factor, could be used to generate a color change threshold to determine whether a given UV-C dose (e.g.  $1.0 \text{ J/cm}^2$ ) has been surpassed.

#### Supplementary Note 4: Assessing specificity of PCIs to germicidal UV-C

Given that ultraviolet decontamination efficacy depends on wavelength, it is critical that PCIs used for UV-C decontamination are not only sensitive, but also specific to germicidal UV-C wavelengths (200-280 nm)<sup>15</sup>. Although low-pressure mercury sources are often denoted as ‘monochromatic’ at 254 nm, they emit several additional peaks in the UV-B-to-visible range<sup>16</sup> that could lead to overestimation of UV-C dose without UV-C-specificity. In order to assess the sensitivity of PCIs to non-germicidal wavelengths, we measured the color change after exposure through a longpass (>300 nm) optical filter. We observed that while PCI1 underwent negligible color change under the longpass filter, PCI2 changed color considerably, with ~10% of the color difference attributable to non-germicidal UV wavelengths (**Supplementary Figure S4(a)**). Sunlight (which contains UV-A and UV-B, but no longer contains UV-C at the earth’s surface<sup>17</sup>) also induced rapid color change ( $\Delta E \sim 28$  in 5 minutes) of PC2, while PC1 only marginally changed ( $\Delta E \sim 1.5$ ) (**Supplementary Figure S4(b)**). These results highlight the importance of specificity to UV-C measurement tools, as common UV-C sources (e.g., low and medium pressure mercury bulbs, LEDs) vary in their proportional outputs within the germicidal UV-C range<sup>18</sup>. Misreporting the germicidal dose could have wide-ranging negative consequences, so it is essential to accurately assess dose in the germicidal range.

## Supplementary Note 5: Radiometer correction factor determination

The OAI radiometer was calibrated using a collimated source such that the sensor is situated a specified distance from the source, at normal geometry (i.e., perpendicular to the optical axis). In this study, however, the sensor is used to measure light that is uncollimated and at non-normal geometric configuration. Since the sensor assembly consists of a cylindrical case where optical elements such as diffusers, filters, apertures are stacked in front of the photosensing element, the offset distance from the front aperture to the photosensing element causes positional sensitivity when applied to uncollimated beams. Light rays with a high angle of incidence may be blocked from reaching the sensing element. Therefore, we anticipate that the irradiance reported by the photosensing element may be lower than the actual irradiance at the sensor's front surface, and correction or calibration needs to be performed to compensate for the sensor's nonideal (non-cosine) angular response.

The inaccuracy in irradiance measurement could be corrected experimentally by calibrating the sensor in the exact conditions for which it will be used; however, in the absence of a reference sensor with an ideal cosine angular response with a photosensing element at the exact same height as the radiometer's photosensing element, this is not possible. Furthermore, because this calibration must be conducted within each specific UV-C system (since systems are frequently sold separate from radiometers), this experimental approach is not practical to the majority of users. Instead of performing this calibration experimentally, this sensor 'calibration' can be performed virtually with the use of optical modeling software to determine spatially dependent 'correction factors' that quantify the amount by which the sensor underestimates true irradiance. The sensor's irradiance readings can then be multiplied by the appropriate correction factor to more accurately reflect the true irradiance.

Colleagues at NIST modelled our specific UV-C source and sensor in Zemax OpticStudio Pro (Version 19.4 SP2). The UV-C bulbs were simulated using known radiation patterns of T8 bulbs. The radiometer was simulated using known physical characteristics of the actual sensor such as the height of the aperture and the angular response of the photodetector, which were furnished by the manufacturer. Monochromatic spectral bandpass at 254 nm was assumed. Since the angular response was only measured up to an angle of incidence of 55°, the response to angles >55° was extrapolated using a Gaussian fit in Labview. The virtual sensor was validated by first comparing its angular response to a simulated collimated light beam at different angles of incidence to the normalized angular response provided by the manufacturer of the radiometer, and then comparing the spatially-resolved normalized virtual irradiance estimates with those of the physical sensor (**Supplementary Figure S5(a)**). As shown in **Supplementary Figure S5(a)**, the ratios of the virtual and physical normalized irradiances are close to one, as expected.

The correction factor is calculated as the ratio of the total irradiance at the front surface of the sensor to the irradiance reported by the physical sensor. The total irradiance from the six bulbs at the plane of the radiometer sensor front surface was mapped across the treatment plane. The virtual sensor was then positioned at various points on that same plane to map what the actual sensor readings would be. The resulting correction factor map is shown in **Supplementary Figure S5(b)**. The values of the correction factor vary from 2.72-3.57 and are spatially-dependent, with larger correction factors required around the periphery of the treatment plane. The corrected and uncorrected radiometer readings were compared to readings from another radiometer with near-ideal (cosine) angular response, as well as compared to simulation. Absolute irradiance readings between the corrected first radiometer and near-ideal cosine second radiometer agreed within 11% (**Supplementary Figure S8(a)**). Furthermore, even though the simulated irradiance map underestimates the extent of nonuniformity present in the treatment plane, the relative nonuniformities measured by the virtually-corrected radiometer agreed within 3% with those measured by the radiometer with near-ideal cosine response (**Supplementary Figure S8(c)**).

The spatially-resolved relative uncertainty was calculated as square root of the sums of the squared relative uncertainties on (1) the OAI calibration (reported by the manufacturer as 3%), (2) the UV-C treatment system's irradiance ray trace standard uncertainty (standard deviation of  $n = 4$  ray traces), (3) the solid angle uncertainty, represented as the relative difference between the virtual and physical sensor readings (similar error is depicted in **Supplementary Figure S5(a)**), and (4) the detector area, represented as the relative difference between the virtual and physical sensor readings under a small aperture (to limit the angles of incidence to near-normal). This spatially-resolved relative uncertainty is shown in **Supplementary Figure S5(c)**. The relative error on the detector area was



estimated as the relative error on the differences between the virtual and physical OAI sensor readings during a validation experiment using a mask/aperture setup described in **Supplementary Note 6**.

The reported correction factors are only accurate for the specific conditions assumed for this virtual sensor calibration. Changes to the physical chamber, sensor or bulb properties, as well as changes to the height and/or angle of the sensor within the treatment system require revised simulations that account for these new conditions. In addition, changes to the sensor such as blockage of the effective aperture or insertion of optical elements are significant changes not accounted for in the simulation and require recalculation of the correction factors. However, changes to the lamp irradiance as lamps age or are replaced are expected; sensor readings will reflect such changes and the calculated correction factors should still apply.

## Supplementary Note 6: Correction factor validation using a mask/aperture setup

To validate the computed correction factors, a mask/aperture setup was used to limit the angular distribution of rays that reach the sensor to verify that the virtual sensor matches that of the actual sensor in positional sensitivity. The mask/aperture setup used a black cardstock-lined cardboard insert to block all emitted UV-C light within the treatment system except for a precisely positioned  $\frac{1}{4}$ " aperture. The virtual calibration was repeated with only one source bulb. A mask containing a  $\frac{1}{4}$ " diameter aperture was simulated directly below and centered on the virtual bulb. This mask/aperture setup for the experimental setup was mimicked using cardboard, black cardstock, and an Iris Diaphragm (M-ID-1.0, Newport) with aperture set to  $\sim\frac{1}{4}$ " diameter. All but 2 bulbs were removed from the physical UV-C source (2 bulbs were required for operation). The mask/aperture was arranged in the UV-C treatment system such that the aperture was centered directly below one bulb and the mask bolstered using popsicle sticks kept vertical using sticky tack. In order to minimize contributions of the second bulb to the irradiance measurements, a strip of black cardstock was vertically affixed to the side of the aperture in between the two bulbs. Minimal crosstalk was validated as  $\leq 0.01$  mW/cm<sup>2</sup> difference in irradiance measured at equidistant offsets from the sensor position below the aperture perpendicular to the long axis of the UV-C treatment plane.

The experiment was conducted by measuring the irradiance detected by the physical sensor both directly normal to the aperture and laterally offset by 1" at several known distances from the bulb and comparing the ratio of these measurements to those predicted by running the equivalent simulation in Zemax OpticStudio. The results are shown in **Supplementary Figure S6**. To further validate the correction factor, PCIs were exposed in the modified mask/aperture setup (in which the correction factor is approximately 1), and the dose-response curve was compared to the curve generated in the original UV-C setup. The results are shown in **Supplementary Figure S7**. While we do not observe perfect agreement between the dose-responses, some variation is expected due to the drastically different irradiances ( $\sim 0.10$  mW/cm<sup>2</sup> under the aperture;  $\sim 7.5$ - $12$  mW/cm<sup>2</sup> without the aperture) measured in the two setups (PCI response as characterized by the manufacturer has some dependence on irradiance<sup>19</sup>).

## **Supplementary Note 7: Nonuniformities in and between UV-C sources necessitate rigorous UV-C dose characterization**

As irradiance is dependent on myriad factors (e.g., UV-C source and surrounding physical environment, operating temperature, bulb conversion efficiency and warm-up status<sup>20,21</sup>), we hypothesized that irradiance variability within and between UV-C treatment systems would necessitate full in-process (vs. snap-shot) validation. To test this hypothesis, we studied two UV-C systems with the same specifications: a Spectroline HCL-1500 with BLE-1T155 15W 254 nm low-pressure amalgam bulbs (System 1), and a Spectroline Spectrolinker XL-1500 with third-party BLE-1T155 15W 254 nm low-pressure mercury bulbs (System 2) (Figure 5(b) of main text, and **Supplementary Figure S12(a)**). Quantification of warm-up times (irradiance rise times), and output degradation over time are presented in **Supplementary Figure S12(b)**. We observed distinct temporal irradiance variation as well as different maximum output ( $\sim 11$  mW/cm<sup>2</sup> vs.  $\sim 7.7$  mW/cm<sup>2</sup>), despite these systems having the same specifications. These irradiance variations propagate to the critical UV-C dose. To extrapolate the effect these differences would have on N95 decontamination protocols, exposure times required to reach the marginally-acceptable 1.0 J/cm<sup>2</sup> dose at the center of the treatment plane were calculated for (i) the two near-identical systems, (ii) whether the bulbs are warmed-up prior to measurement, and (iii) whether the calculation is performed from measurements at the beginning or end of the exposure (**Supplementary Figure S12(c)**). For System 1 after sufficient bulb warm-up, the average times required to deliver 1.0 J/cm<sup>2</sup> dose only differed by 1.5% if calculated from the irradiance measured at the start and end of the exposure, indicative of relatively stable output over the treatment period. In contrast, the calculated average times to deliver the same dose in the same system without sufficient bulb warm-up differed by 29% (**Supplementary Figure S12(c)**, top row), highlighting the importance of rigorously controlled bulb warm-up protocols. Following a similar trend, the calculated average times to deliver 1.0 J/cm<sup>2</sup> without sufficient bulb warm-up for System 2 also differed by 29%. However, the absolute time required for System 2 to deliver 1.0 J/cm<sup>2</sup> dose is far less than System 1 due to higher absolute irradiance. In contrast to System 1, the average times calculated to deliver 1.0 J/cm<sup>2</sup> dose from the irradiance measured at the start and end of the exposure in System 2 after sufficient bulb warm-up still differed by 23% (**Supplementary Figure S12(c)**, bottom row). This difference is due to an observed decline in irradiance over time, which we hypothesize is caused by the increased sensitivity to temperature of low-pressure mercury bulbs compared to low-pressure amalgam bulbs<sup>22</sup>.

## References

1. Brian Heimbuch, Del Hamish. *Research to Mitigate a Shortage of Respiratory Protection Devices During Public Health Emergencies*.  
[https://www.ara.com/sites/default/files/MitigateShortageofRespiratoryProtectionDevices\\_2.pdf](https://www.ara.com/sites/default/files/MitigateShortageofRespiratoryProtectionDevices_2.pdf) (2019).
2. Lore, M. B., Heimbuch, B. K., Brown, T. L., Wander, J. D. & Hinrichs, S. H. Effectiveness of Three Decontamination Treatments against Influenza Virus Applied to Filtering Facepiece Respirators. *Ann. Occup. Hyg.* **56**, 92–101 (2011).
3. Heimbuch, B. K. *et al.* A pandemic influenza preparedness study: Use of energetic methods to decontaminate filtering facepiece respirators contaminated with H1N1 aerosols and droplets. *Am. J. Infect. Control* **39**, e1–e9 (2011).
4. Larason, T. & Ohno, Y. Calibration and characterization of UV sensors for water disinfection. *Metrologia* **43**, S151–S156 (2006).
5. Larason, T. C. & Cromer, C. L. Sources of error in UV radiation measurements. *J. Res. Natl. Inst. Stand. Technol.* **106**, 649 (2001).
6. ASTM Standard D2244-16. Standard Practice for Calculation of Color Tolerances and Color Differences from Instrumentally Measured Color Coordinates. *ASTM Int.* (2016) doi:10.1520/D2244-16.
7. Solari, F., Girolimetti, G., Montanari, R. & Vignali, G. A New Method for the Validation of Ultraviolet Reactors by Means of Photochromic Materials. *Food Bioprocess Technol.* **8**, 2192–2211 (2015).
8. Cui, G., Luo, M. R., Rhodes, P. A., Rigg, B. & Dakin, J. Grading textile fastness. Part 1; Using a digital camera system. *Color. Technol.* **119**, 212–218 (2003).
9. Nixon, M., Outlaw, F., MacDonald, L. W. & Leung, T. S. The importance of a device specific calibration for smartphone colorimetry. *Color Imaging Conf.* **2019**, 49–54 (2019).
10. Luo, M. R., Cui, G. & Rigg, B. The development of the CIE 2000 colour-difference formula: CIEDE2000. *Color Res. Appl.* **26**, 340–350 (2001).
11. Gómez-Polo, C. *et al.* Comparison of the CIELab and CIEDE2000 color difference formulas. *J. Prosthet. Dent.* **115**, 65–70 (2016).
12. Luo, M. R. CIEDE2000, History, Use, and Performance. in *Encyclopedia of Color Science and Technology* (ed. Luo, M. R.) 202–207 (Springer New York, 2016). doi:10.1007/978-1-4419-8071-7\_7.
13. Mills, A., McDiarmid, K., McFarlane, M. & Grosshans, P. Flagging up sunburn: a printable, multicomponent, UV-indicator that warns of the approach of erythema. *Chem. Commun.* 1345 (2009) doi:10.1039/b900569b.
14. El Seoud, O. A., Baader, W. J. & Bastos, E. L. Practical Chemical Kinetics in Solution. in *Encyclopedia of Physical Organic Chemistry, 5 Volume Set* (ed. Wang, Z.) 1–68 (John Wiley & Sons, Inc., 2016). doi:10.1002/9781118468586.epoc1012.
15. Kowalski, W. *Ultraviolet Germicidal Irradiation Handbook: UVGI for Air and Surface Disinfection*. (Springer Berlin Heidelberg, 2009). doi:10.1007/978-3-642-01999-9.
16. Schmid, J., Hoenes, K., Rath, M., Vatter, P. & Hessling, M. UV-C inactivation of *Legionella rubrilucens*. *GMS Hyg. Infect. Control* **12**, 1–6 (2017).
17. CDC. Ultraviolet Radiation. <https://www.cdc.gov/nceh/radiation/ultraviolet.htm> (2019).
18. Kowalski, W. *Ultraviolet Germicidal Irradiation Handbook: UVGI for Air and Surface Disinfection*. (Springer Berlin Heidelberg, 2009). doi:10.1007/978-3-642-01999-9.
19. Stefan Källberg. *UVC exposure (254 nm) of UV sensitive material at different irradiation levels*. [http://intellego-technologies.com/wp-content/uploads/2020/05/RISE\\_report\\_Intellego\\_UVCdoimeter\\_100.pdf](http://intellego-technologies.com/wp-content/uploads/2020/05/RISE_report_Intellego_UVCdoimeter_100.pdf) (2017).

20. Lawal, O. *et al.* Method for the Measurement of the Output of Monochromatic (254 nm) Low-Pressure UV Lamps#. *IUVA News* **19**, 9–16.
21. ASTM International. *Standard Test Method for Determining Antimicrobial Efficacy of Ultraviolet Germicidal Irradiation against Influenza Virus on Fabric Carriers with Simulated Soil*. <https://compass-astm-org.libproxy.berkeley.edu/download/E3179.35883.pdf>.
22. Lister, G., Lawler, J., Lapatovich, W. & Godyak, V. The physics of discharge lamps. *Rev. Mod. Phys.* **76**, 541–598 (2004).